GENERAL ATOMICS

March 27, 2007

Mr. Larry L. Sutton
Senior Subcontract Administrator
Princeton University
Princeton Plasma Physics Laboratory (PPPL)
P.O. Box CN-17
Princeton, New Jersey 08543
ATTN: Subcontract S006962-F

Reference: **Study to Assess the Design of the ITER Divertor Interferometer**
Subcontract S-006962-F
under Prime Contract No. DE-AC02-76CH03073
GA Project 30279

Dear Mr. Sutton:

In accordance with the requirements of the referenced contract, enclosed herewith is one copy of the document listed below:

GA REPORT	TITLE
GA-C25756	**DESIGN ASSESSMENT OF THE DIVERTOR INTERFEROMETER** **Conceptual Design** **Final Report**

If you have any questions or comments, please do not hesitate to contact me by telephone at 858.455.3057, at FAX 858.455.3545 or by E-mail at Ramona.Gompper@gat.com.

Sincerely,

R Gompper

Ramona Gompper
Sr. Contract Administrator
Enclosure: As Stated

GA–C25756

DESIGN ASSESSMENT OF THE DIVERTOR INTERFEROMETER CONCEPTUAL DESIGN

Final Report

by
PROJECT STAFF

Prepared under
Contract No. S006962-F
for Princeton Plasma Physics Laboratory

DATE PUBLISHED: MARCH 2007

GENERAL ATOMICS

GA–C25756

DESIGN ASSESSMENT OF THE DIVERTOR INTERFEROMETER CONCEPTUAL DESIGN

Final Report

by
PROJECT STAFF

Prepared under
Contract No. S006972-F
for Princeton Plasma Physics Laboratory

GENERAL ATOMICS PROJECT 30279
DATE PUBLISHED: MARCH 2007

GENERAL ATOMICS

ABSTRACT

In the harsh environment of the divertor region in ITER, plasmas spanning a huge density range from 10^{19} to 10^{22} m^{-3} are anticipated making measurement of the plasma density particularly challenging. Various interferometer techniques are assessed for application to the ITER divertor region. Without re-engineering the divertor cassette to increase the toroidal gap space allotted for the measurement, a conventional two-color CO_2 (10.6/5.3 μm) interferometer provides an attractive option for divertor density measurement. ITER specifications of 20% phase resolution, 1 ms time response and 5 cm spatial resolution can all be achieved. Refraction is negligible at this wavelength and various means for dealing with potential fringe counting errors are identified. Realtime alignment and the use of corner-cube retro-reflectors are deemed necessary to maintain alignment. Mirror degradation can be minimized through temperature control and a recessed design of plasma facing components.

TABLE OF CONTENTS

LIST OF FIGURES

LIST OF FIGURES (continued)

LIST OF TABLES

1. INTRODUCTION

One of the ITER diagnostic systems being provided by the US is the Divertor Interferometer. This system consists of a multichannel array along both the inner and outer divertor legs to contribute to the measurement of the electron density in the divertor region. Currently, six observation channels are planned for the outer leg and four for the inner. Each channel will measure the line integral of the density along its line of sight continuously. The spacing of the different channels will provide spatial information along the legs. It is desirable to obtain higher resolution, particularly in the region adjacent to the strike points.

Access to the divertor region in a large tokamak is difficult and only a few attempts to make interferometer measurements in this region have been made. An RF, two-color system operating at 130/200 GHz was built for the Joint European Torus (JET) tokamak [1] and operated with some limited success. A 250 GHz RF system was built for the DIII-D tokamak [2] but it suffered from loss of signal due to strong refraction effects. High-density gradients in the divertor due to high recycling and edge localized modes (ELMs) prevented continuous fringe measurements and the density information was lost. Refraction effects were much more severe than those calculated from simple estimates.

Interferometry measures the refractive index of the plasma integrating along its optical path. The phase change is linearly proportional to the plasma density and the probing wavelength. A list of plasma parameters in the divertor accessible to this technique and the associated ITER measurement requirements are given in Table I. Measurement 41, shown in Table I, has to cover a very wide dynamic range of densities. Specifications given for this measurement are density range from 10^{19} to 10^{22} m^{-3}, and density resolution of 20% accuracy. Time response of 1 ms, and spatial resolution of 5 cm [3] along the leg and 3 mm across the divertor leg are also specified [4]. The typical plasma path length for a probing beam will be a few centimeters. Spatial resolution across the leg is not possible by interferometry and the required spatial resolution along the leg is only achievable if there are closely spaced channels. However, good time resolution is feasible and interferometry will be used in conjunction with the planned pulsed Thomson scattering system to provide the necessary quality of data. Realtime density output is not mentioned but presumed necessary for ITER operations.

Table I
Extracted From Requirements for Plasma and First Wall Measurements: Parameter Ranges, Target Measurement Resolutions and Accuracy Included in the Plant Integration Document – June 2004

Measurement	Parameter	Condition	Range or Coverage	Resolution		Accuracy
				Time or Frequency	Spatial or Wave No.	
41 Divertor electron parameters	n_e		$1x10^{19}$-$1x10^{22}/m^3$	1 ms	50 mm along leg, 3 mm across leg	20%
36 Plasma parameters at the divertor target	n_e		$1x10^{18}$-$1x10^{22}/m^3$	1 ms	3 mm	30%
14 H-mode: ELMs and L-H transition indicator	ELM density transient		r/a > 0.9	TBD	TBD	TBD
16 Divertor operational parameters	Position of the ionization front		0-TBD m	1 ms	100 mm	—

Challenges for measuring density in ITER divertor plasmas are the large density dynamic range, harsh environment and limited space. In addition, there are four other areas where the divertor interferometer density measurement can provide information in support of other divertor diagnostic measurements. These include:

- measurement of density at the divertor target expected to be determined by probes at the surface of the target
- measurement of large-amplitude, fast, transient events associated with ELM instabilities
- the divertor will necessarily frequently have to operate with the plasma detached from the target surface, and the position of the highly radiating zone must be known
- measurement of MARFEs, localized high density plasma formations that may also drift into or form in the divertor interferometer lines-of-sight

Both of these last two requirements will be supplemented by endoscopic imaging and spectroscopic methods. The primary engineering constraint is the envisioned small 1-2

cm space in the toroidal gap between divertor cassettes that is available to make the measurement.

The ITER International Team has allocated locations on either side of divertor cassette #22 located at port L8 for the interferometer system. It may share the port with the uncredited laser induced fluorescence system. The front-end components nearest the plasma of the interferometer will be mounted to the sides of the flexible divertor cassette shown in Fig. 1.

(a)

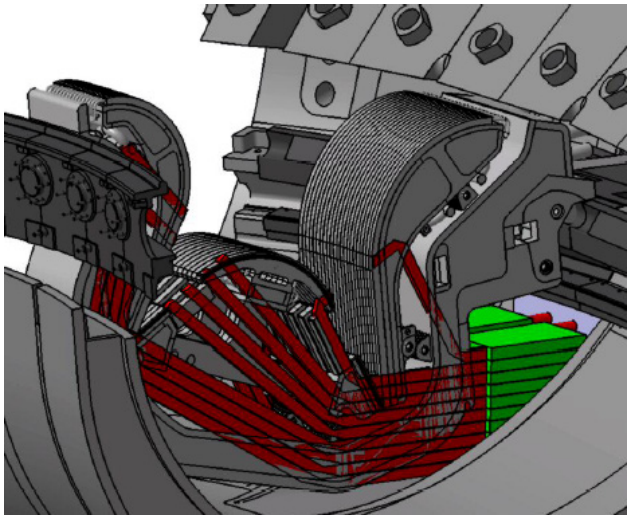

(b)

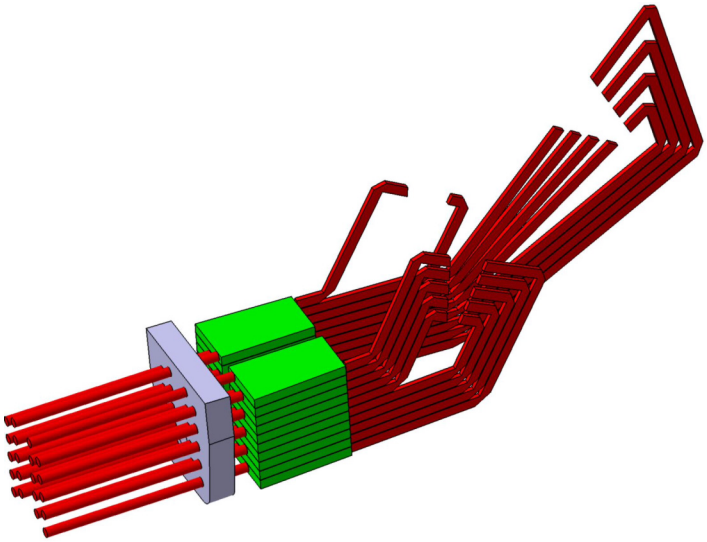

Fig. 1. The ITER diagnostic cassette design showing potential interferometer sightlines (or waveguides). The cross-section for each is 20x40 mm. (b) same as (a) but (rotated and) showing interferometer sightlines only for both sides of the cassette. 4 chords on inner leg and 6 on outer divertor leg.

The anticipated electron density distribution for a standard ITER discharge scenario is shown in Fig. 2, where the density profile is provided for eight different lines of sight along the outer divertor leg. The maximum density is expected to occur along Path 2 ($1.8x10^{21}$ m^{-3}) and minimum along Path 8 ($1.8x10^{20}$ m^{-3}). A minimum density of $\sim 10^{19}$ m^{-3} would then occur near the wall. Divertor path lengths are relatively short and vary from 0.05 m (Path 2) to 0.45 m (Path 8). For purposes of this conceptual design study, we will take this discharge scenario [covering from $1x10^{19}$ m^{-3} divertor edge (or wall) to $1.8x10^{21}$ m^{-3} central divertor] as the baseline for designing the interferometer system. This discharge corresponds to an ITER divertor case with 75 MW into the scrape-off layer (SOL). For the maximum density put forward in the ITER design specifications, we will simply scale each profile by a factor of ~5 so that the peak density along Path 2 reaches 10^{22} m^{-3}. On this basis, the local density distributions shown in Fig. 2 can be converted into line integrals along each sight line for both the ITER divertor baseline and maximum density cases, as shown in Fig. 3.

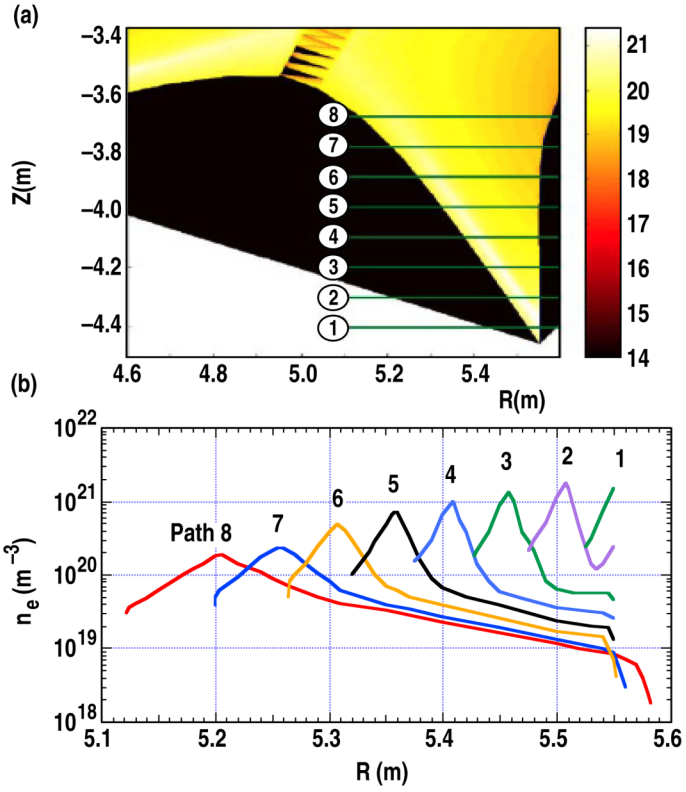

Fig. 2. Modeled density distribution for the outer divertor leg for the baseline discharge scenario. Peak density in Path 2 is $1.8x10^{21}$ m^{-3}.

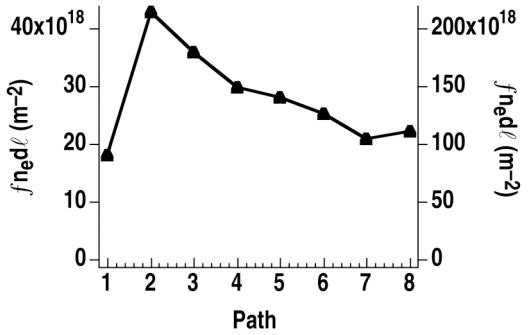

Fig. 3. Estimated line-integrated densities for optical Paths 1 through 8 (Fig. 1) for the ITER baseline case — 1.8×10^{21} m^{-3} peak density for Path 2 (left vertical axis) and high density case — 1×10^{22} m^{-3} peak density for Path 2 (right vertical axis).

2. OPTICAL PATH DESIGN

The space constraints in the divertor of ITER are extremely limiting. Only a 1-2 cm toroidal gap between divertor cassettes for access is presently envisaged. Waveguide systems inside the divertor cassette were investigated but it was felt that system alignment could not be maintained with sufficient precision to insure significant transmission [5]. Alignment difficulty results largely from movement of optical components due to thermal expansion. For a waveguide transmission system, it is critical that the beam stay on axis to minimize transmission losses and maintain polarization integrity (important for polarimetry measurements). Additionally, with respect to interferometry, to compensate for path length changes two wavelengths will be required for the frequencies of interest. The use of a multimode waveguide system may result in the two wavelengths taking slightly different paths leading to incomplete vibration compensation. For free space propagation, one only need keep the source and signal beams on the optical components. This simplifies realtime feedback alignment requirements and has led us to investigate such systems. In addition, a double pass setup using corner cube reflectors (CCR) for the return beam is deemed necessary to maintain optical alignment. Although a free space solution for CO_2 laser beams in the divertor region was found, it is recommended to continue to explore waveguide solutions because of the potential access advantages they provide.

Free space Gaussian beam analysis of diffraction limited CO_2 lasers beams at 10.6 μm indicate that the beam diameter can be <6.4 mm for distances of 4.5 m when the beam waist is relayed to the CCR by a focusing mirror 1.5 m from the CCR as shown in Fig. 4 (beam waist diameter of 4.46 mm at the CCR). At 57(118) μm these diameters increase to 14.3 (21.4) mm. For proper beam propagation, the clear aperture of the optics should be at least two times larger than the beam diameter. This makes the optics for the 57 and 118 μm systems larger than the allotted space in the toroidal gap (<2 cm). Therefore, the use of 10.6 μm is attractive from the standpoint of access. Note that real laser beams will not necessarily be diffraction limited and the beam diameters may be larger than these estimates. If longer wavelengths such as 57 or 118 μm were chosen, extensive prototyping of waveguide at appropriate frequencies and path lengths would be required. Sensitivity of beam polarization integrity (for Cotton Mouton polarimetry), transmitted power and mode quality to misalignment must be thoroughly examined as well as the effects of waveguide propagation on vibration cancellation in two-color systems.

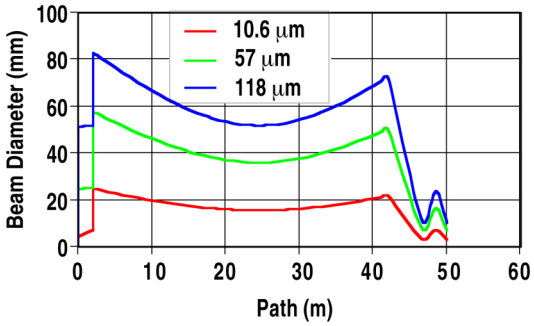

Fig. 4. Beam diameter vs. path length using an off-axis parabola mirror to relay the beam waist the last 3 m. Path = 0 corresponds to the diagnostic hall where the radiation source is located and Path = 50 m represents the location of the CCR for a double pass interferometer system.

A CCR with dimensions 15 mm x 25 mm could fit in the gap and handle the CO_2 laser beam size. The CCR is extended in the vertical direction so that the incoming and return beams do not overlap (Fig. 5). Return beam offset is approximately 1.5 cm. This configuration would allow for minimum channel spacing (spatial resolution) of 3 cm along the divertor leg which meets the ITER specification of 5 cm. Interferometry measurements are line-integrated thereby providing no spatial resolution across the divertor leg. Since there are no vertical obstructions in the toroidal gap, there is space for 20-25 chords for each divertor leg. The total number of channels actually selected will most likely be limited by available space for incoming/return beams.

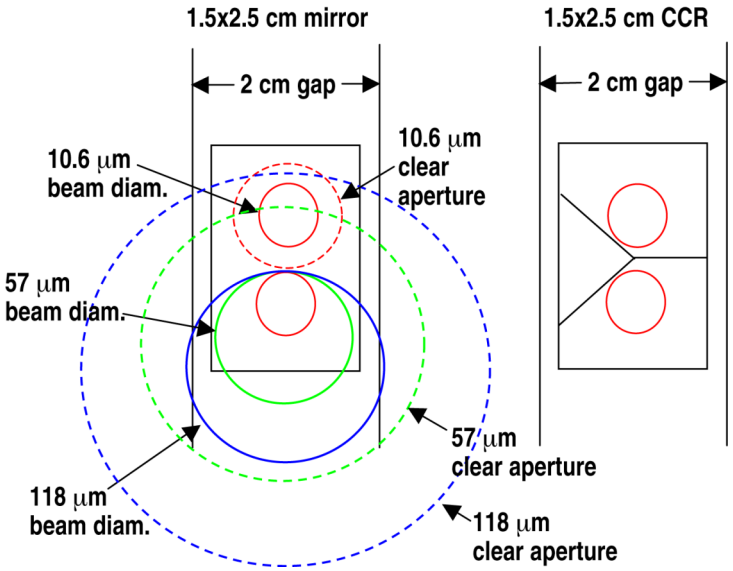

Fig. 5. 1.5x2.5 cm mirror (left) and CCR (right) in the 2 cm gap between divertor cassettes. The 0.5 cm footprint of the input and return CO_2 laser beams are shown as red circles. The relative size of the 57 and 118 μm beams are shown as green and blue circles respectively. The dashed circles are the required clear apertures to preserve good beam characteristics.

An optically efficient design suggested by G. Vayakis [6] uses a curved (convex) mirror to produce a fan of beams from a single sheet laser beam as shown in Fig. 6. This fan beam would then illuminate an array (<25 for each leg) of closely spaced (~3 cm) CCRs. Separate CCRs for each chord reflect portions of the beam back on themselves. This may result in a portion of the return beam re-entering the laser and causing instabilities unless appropriate isolation techniques are employed. Separating the various chords from each other would most likely require an imaging system [7].

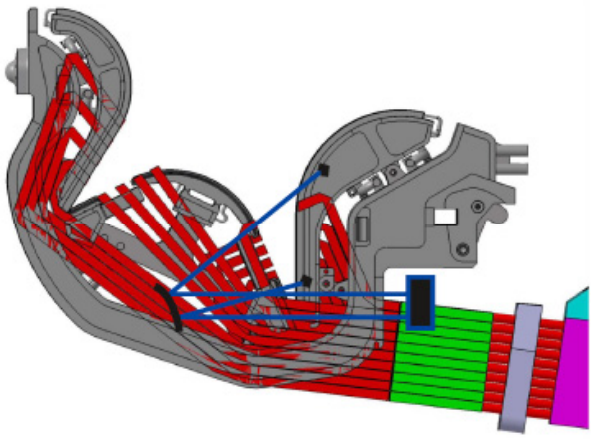

Fig. 6. Lines of sight (blue) from a sheet laser beam distributed into a fan by a curved mirror. CCR are used to define the chords (two extremes shown) and reflect the beams back on themselves. From [6].

Disadvantages of an imaging system include (1) common point of failure (i.e., one laser and one set of optics), (2) large optics have more exposure to the plasma and would be subject to more degradation. An interferometer system employing discrete chords/optics can use multiple sources and receivers providing a safety net in the event of component failure. In addition, discrete chords can employ long, small aperture tubes along each sightline which will significantly decrease the solid angle exposure to plasma.

In a variation of this design, separate laser beams are used for each chord and only a subset of the total number of CCRs need be populated for any given discharge [4]. A possible layout implementing this type of configuration is shown in Fig. 7, where ten and six chords with a 5 cm vertical spacing (red lines) are shown to scale on the outer and inner divertor legs, respectively. Such a system has the advantage of being flexible, that is, one could choose to populate a small number of available CCRs focusing on the expected height of the strike point. Minimum chord spacing would be limited by the CCR size of 3 cm. Optionally, one could choose a smaller number of fixed chords with less dense spacing to span the entire divertor leg while reducing the overall system requirements in terms of number of lasers, demodulation software, etc.

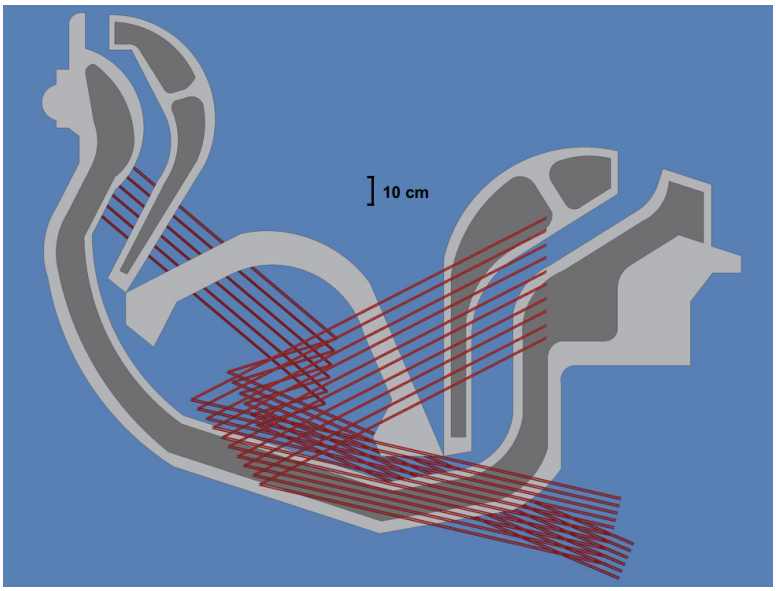

Fig. 7. Possible layout for ten CO_2 laser chords on the outer divertor leg and six on the inner leg. Each chord consists of a ~0.5 cm diameter input beam and a ~0.5 cm return beam offset vertically by 1 cm. The chords are terminated with retro reflectors and spaced 5 cm vertically. Off-axis parabolic turning mirrors are used to relay the laser beam waist to the retro reflectors.

A closeup of the inner and outer legs is shown in Fig. 8. Each chord consists of two ~0.6 cm diameter beams, with the return beams offset in the vertical direction due to 2 cm size constraints in the toroidal direction. Off-axis parabolic mirrors are used under the dome of the divertor to relay each laser beam waist to the CCR. Note that making the measurements at longer wavelengths requires increasing CCR size and reducing total number of possible chords. Mirror damage can be mitigated by placing mirrors behind long, high aspect ratio shield tubes and controlling their temperature to minimize deposition. The free space optical system permits the possible change of wavelengths at a later time and the use of laser blow-off to clean the mirrors.

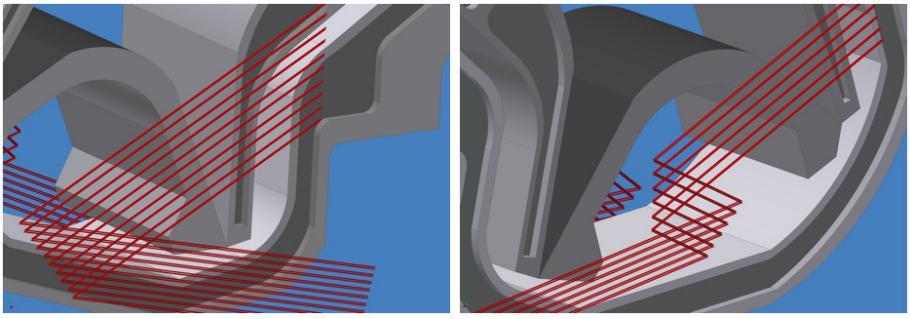

Fig. 8. Close-up view of inner and outer divertor legs from Fig. 7.

3. MEASUREMENT TECHNIQUE

3.1. Method and Wavelength Selection

The 2005 conceptual design report [8] reviews three possible interferometer configurations: conventional two-color CO_2 based interferometer (10.6 μm); the Cotton-Mouton interferometer (FIR 57 or 118 μm); and differential interferometer [9] (10.6 μm). There are other options as well with each having different capabilities and limitations. Below, in Table II, we provide an overview of these options and explore applications to the ITER divertor in the discussion that follows.

Table II
Potential Interferometry and Polarimetry Techniques
That Can Be Applied in the ITER Divertor

Interferometer Technique	Fringe Skip	1 ms Time Response	Accuracy 20%	Calibration Required	Realtime Alignment	Refraction Effect	Fit 2 cm Toroidal Gap
Two-color (10.6 and 56.3 μm) int.	Possible	Yes	Yes	No	Yes	Small	Yes
Cotton-Mouton (118 μm)	No	Yes	Yes	Yes	Yes	Possible — ELMs or MARFEs	No
Faraday rotation (57 and 118 μm)	No	Yes	Yes	Yes	Yes	Possible — ELMs or MARFEs	No
Differential interferometer (10.6 μm)	No	Yes	Yes	Yes	Yes	Small	Yes
Dispersion interferometer (10.6 μm)	Unlikely	Yes	Yes	No	Yes	Small	Yes

It should be noted that each measurement technique evaluated can be designed for fast time response (~1 μs) which would allow fast transient events, like ELMs, to be resolved.

3.1.1. Two-Color Interferometer

In general, a two-color interferometer (10.6/5.3 μm, 57/48 μm, or 118/57 μm) can provide a density measurement in divertor for the range 10^{19}-10^{22} m^{-3}, as described previously [6]. The path lengths are short (5 to 50 cm) so that beam displacement due to refraction appears manageable, even at long wavelengths like 118 μm (Sec. 3 and

Appendix A for more detailed refraction discussion). However, like the ITER Tangential Interferometer Polarimeter (TIP) system, implementing a two-color technique by itself (at any wavelength) leaves a potential for fringe skip errors. For long pulse discharges such as those anticipated for ITER (~400 s), the density measurement capability is potentially lost as soon as a fringe counting error occurs. This will most likely be the case during large and fast transient events like ELMs and MARFEs or even due to thermal expansion. Consequently, the reliability of density measurement remains a challenge.

The estimated single-pass phase shifts for 118, 57 and 10.6 μm laser radiation, shown in Fig. 9, are calculated from the simulated density profiles provided in Fig. 2. At wavelengths 57 and 118 μm, the plasma-induced phase is always much greater than a single fringe. However, the phase shift at 10.6 μm is always of order or less than 2π (Fig. 10). This potentially makes it easier to recover from the temporary loss of signal because there would not be ambiguities due to multiple plasma-induced fringes. For instance, as will be discussed later, the use of a second harmonic or dispersion interferometer at 10.6 μm could eliminate vibration/thermal expansion fringes entirely and make the density signal completely unambiguous as long as the plasma phase shift remains less than 2π (more discussion on this in Sec. 3.2.5).

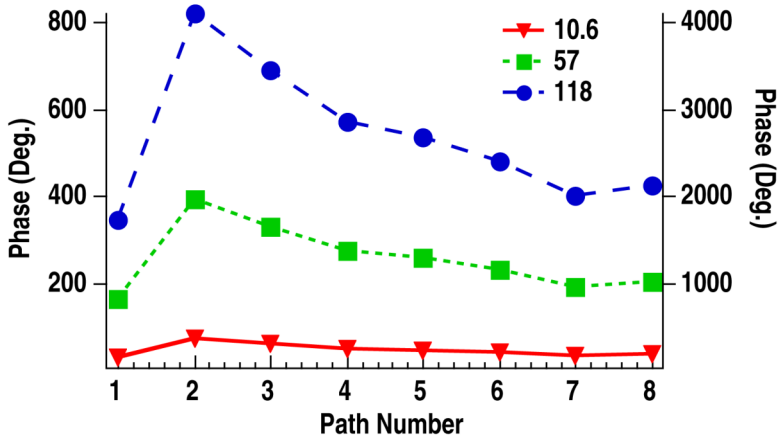

Fig. 9. Estimate of single-pass interferometer phase shift at 118 (long dashed line), 57 (short dashed line) and 10.6 μm (solid line) for the ITER baseline case — 1.8×10^{21} m^{-3} for Path 2 (left vertical axis) and high-density case — 1×10^{22} m^{-3} for Path 2 (right vertical axis).

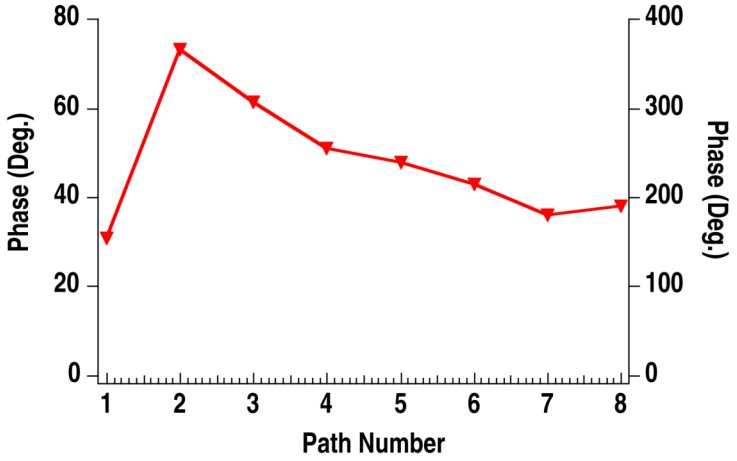

Fig. 10. Expanded view of Fig. 9, showing 10.6 μm phase shift.

Resolution. The resolution of a two-color vibration compensated interferometer depends on the phase noise (usually 1-3 degrees) and the difference in wavelength between the two colors. Table III shows the resolution of various combinations of wavelengths for a 1-degree phase measurement error. The resolution is given approximately by the analytic formula

$$\delta n_e L = \frac{\delta\phi}{r_e(\lambda_1 - \lambda_2)} \quad , \tag{1}$$

where r_e is the classical electron radius and $\delta\phi$ is the phase measurement error. The ITER specification for accuracy is 20% of $n_e L$. For the low-density case of $1\text{x}10^{19}$ m^{-3} (as specified in Table I), the long wavelength choices (57/48 and 118/57 μm) and the 10.6/5.3 μm pair meet the desired resolution of $1\text{x}10^{18}$ m^{-2}. If the minimum density is increased to $1\text{x}10^{20}$ m^{-3}, then all the wavelength combinations can provide sufficient accuracy. It should be noted that a double-pass path length of 0.5 m was used for Table III. Depending on which path is selected (Fig. 2), this length can vary from approximately 0.2 to 0.8 m.

Taking the 20% accuracy requirement and applying it to the minimum $n_e L$ of $1.7\text{x}10^{19}$ m^{-2} for the baseline density case shown in Fig. 3, implies a minimum resolvable $n_e L$ of $3.4\text{x}10^{18}$ m^{-2}. This is satisfied by the 10.59/5.3 μm system which is capable of $1.2\text{x}10^{18}$ m^{-2} at 1-degree phase noise (or ~7% of the minimum $n_e L$). In addition, the longer wavelength choices of 57.2/47.6 and 118/57.2 also meet this resolution. The electronics are capable of resolution <0.1 degree if other sources of noise can be controlled. This would lead to less than 1% of the minimum $n_e L$. The CO_2 laser dispersion interferometer on TEXTOR has achieved $2\text{x}10^{17}$ m^{-2} resolution (or ~1% of the

minimum $n_e L$) and 1 ms temporal resolution using averaging techniques [10]. As expected, the longer wavelengths typically have better phase resolution. Although not specified as a requirement for the divertor, real-time density information is also available with any of the above-mentioned systems. The actual use of such information for feedback control will depend on the reliability of the measurements.

Table III
Calculated Two-Color Resolution for Various Wavelength Combinations

λ1 (μm)	λ2 (μm)	Measurement Error (degree)	Path Length (m)	Minimum Density (m^{-3})	Required Resolution (m^{-2})	Calculated $\delta n_e L$ Resolution (m^{-2})
10.59	5.3	1	0.5	$1.0x10^{19}$	$1.0x10^{18}$	$1.2x10^{18}$
10.59	9.27	1	0.5	$1.0x10^{19}$	$1.0x10^{18}$	$4.7x10^{18}$
12.1	9	1	0.5	$1.0x10^{19}$	$1.0x10^{18}$	$2.0x10^{18}$
57.2	47.6	1	0.5	$1.0x10^{19}$	$1.0x10^{18}$	$6.5x10^{17}$
118	57.2	1	0.5	$1.0x10^{19}$	$1.0x10^{18}$	$1.0x10^{17}$

Fringe Rates and Counting Errors. If the total (plasma plus thermal expansion or vibrations) measured phase of an interferometer exceeds 2π, a counter is used to track the number of elapsed 2π segments. If there is an error in the count, a fringe jump occurs and the phase can be in error by some multiple of 2π. (Some systems count phase changes of π/2 instead of 2π.) This presents a significant problem for real-time density control of the plasma since the absolute density information is lost.

Fringe jumps can be due to several different things. The signal may be lost due to refraction effects in the plasma or misalignment of the interferometer due to vibrations or mechanical motion of the mirrors. Refraction effects are proportional to the wavelength and can be mitigated by choosing a short wavelength. Alignment effects can be mitigated by using robust mirror mounts and/or using a feedback alignment system.

Fringe jumps are also due to the phase changing faster than the interferometer system can follow. The fast phase changes can be due to vibration or density. The plasma density change during ELMs, disruptions, and pellet injection are responsible for fast phase changes in many tokamaks. This problem can be mitigated by choosing a high modulation frequency and counting rate for the interferometer.

The fringe jump problem can be avoided in interferometer systems where the expected phase change is less than 2π. This is often true for Faraday and Cotton-Mouton interferometers due to their inherent insensitivity to vibrations, but the use of these

interferometers is not always practical. Likewise, the dispersion interferometer can have phase changes less than 2π with the right choice of wavelength.

In systems where fringe jumps occur, it is possible to recover the correct density information in real-time, in some cases. The phase φ can be recovered if other information is known or assumed such as:

1. φ_{vib} is small during a jump.
2. φ_{nel} is small during a jump.
3. Adjacent channels do not have jumps at the same time.
4. Other density information is available such as Faraday interferometer or Thomson scattering.
5. Refraction only affects the long wavelength in a two-color system.
6. Vibration only affects the short wavelength in a two-color system.

Fringe jump detection can be accomplished by triggering on:

1. A large change in φ_{vib} above a threshold.
2. More than one zero crossing of the signal in a sample time.
3. Signal amplitude reduction below a threshold.
4. Comparison with other measurements.

Once a fringe jump is detected, additional information can be used in a fast algorithm to correct the phase. Assuming φ_{vib} is small, real-time correction of the interferometer phase has been done on the JET [11,12] tokamak with a 60%-80% success rate when the cause of the fringe jumps were due to Type I and Type III ELMs.

For a two-color system with wavelengths λ_1 and λ_2, unambiguous phase determination typically relies on tracking the phase of two interferometers (ϕ_1 and ϕ_2) through multiple fringes — opening up the possibility of fringe skips. It can be shown that within a range $nL/k < \pi$, where $k = |\lambda_2/[r_e (\lambda_2^2 - \lambda_1^2)]|$ and $r_e = 2\text{x}10^{-15}$ m^{-2}, it is sufficient to know the phase of one wavelength system (ϕ_1) precisely and the other (ϕ_2) only within the range $0\text{-}2\pi$; i.e. it is not necessary to count fringes for ϕ_2. This reduces the system's overall susceptibility to fringe skips. For a 10.59/5.27 system this restricts $nL < 7\text{x}10^{19}$ m^{-2}, which is reasonable but not without room for error in the higher density cases shown in Figs. 2 and 3.

The fringe skip issue is an active area of research and remains a problem for two color interferometry. However, utilizing modern digital signal processing techniques in combination with algorithms such as those implemented on the JET tokamak, helps to

mitigate the risk significantly. Additionally, as mentioned earlier, an advantage for the 10.6/5.3 μm wavelength choice is that the plasma-induced phase shift is (nearly) always less than a fringe, a fact that may help significantly if signal loss were to occur.

3.1.2. Faraday Rotation Interferometer

A Faraday rotation interferometer measures a phase directly proportional to $\approx \lambda^2 \int n_e(r,t) B_{||} d\ell$, where $B_{||}$ is the component of the magnetic field parallel to the beam propagation direction. Unlike the TIP system where density measurements can be made independently by simultaneous Faraday rotation and two-color interferometry measurements, the current divertor interferometer design of wave launcher and receiver does not permit the Faraday rotation measurement since the wave propagation direction is perpendicular to toroidal field. If density measurement *reliability* in divertor region is essential for ITER operation (i.e., no fringe counting errors tolerated), by allowing the probe laser beam to have a 1 cm toroidal displacement, a Faraday measurement becomes possible due to the magnetic field component along the laser path. The effect is measurable (depending on wavelength choice) because B_T is large (and known) for ITER. A spatial offset of 1 cm gives a pitch angle of 1.2 degree (for 50 cm path length) to 11 degree (for 5 cm path length). The Faraday rotation angle would vary from 3 degrees to 28 degrees for source radiation wavelength 57 μm at B_T = 6 T with density 10^{21} m^{-3}. Because of the sensitivity to pitch angle, the spatial offset would have to be precisely known and it would have to remain mechanically stable. Also, the poloidal magnetic field component, if any, would have to be known. The rotation angle is well within Faraday rotation phase resolution (<0.1 deg) of existing systems (Note that measured phase is two times Faraday rotation angle). Since the Faraday measurement is not sensitive to vibrations or thermal expansion and the Faraday effect phase shift is $<<2\pi$, no fringe counting errors would occur, even if the signal were temporally lost.

However, even a 1 cm toroidal offset conflicts with the toroidal gap space presently available in ITER designs. It may be possible to implement a 1-deg tilt without modifying with gap width by designing the gap itself with a 1 cm offset. However, as mentioned earlier, use of 57 μm (or longer wavelength) radiation requires more space due to the larger beam size (Sec. 3.1.3, the use of waveguide within the toroidal gap is not deemed feasible). Hence, the toroidal gap would need to be re-engineered to provide the extra space required to make a Faraday measurement. Faraday rotation at shorter wavelengths like 10.6 μm does not appear feasible as the rotation angles are too small with modest (~1 cm) toroidal offset.

3.1.3. Cotton-Mouton Interferometer

A Cotton-Mouton interferometer measures a phase directly proportional to $\approx \lambda^3 \int n_e(r,t) B_\perp^2 d\ell$, where $B_\perp$ is the perpendicular magnetic field that for the case of the ITER divertor, is the known toroidal magnetic field. Using this approach, the total measured phase is always <<2π thereby removing the problem of fringe counting errors. The maximum Cotton-Mouton phase shifts in the divertor region, for the baseline density case (1.8×10^{21} m^{-3}) are in the 2-deg to 4-deg range and for the maximum density case density (~10^{22} m^{-3}) 10-deg to 20-deg for laser radiation at wavelength λ = 118 μm using B_T = 6 T [1,2]. The Cotton-Mouton effect scales as ~$\lambda^3 B_T^2$, resulting in phase shifts that are too small for shorter wavelength operation at 57 or 10.6 μm. Like the Faraday rotation measurement, this approach is insensitive to thermal expansion and vibration effects. A Cotton-Mouton measurement at 118 μm could provide accurate density measurements for the large divertor density dynamic range. Phase resolution <0.1 deg (based on existing systems) would meet the ITER divertor interferometer resolution requirements (20% accuracy) for the baseline and high density cases with minimum $\delta n_e L \sim 1.2 \times 10^{18}$ m^{-2}. For densities <10^{20} m^{-3}, the Cotton-Mouton effect would be too small to meet the resolution specifications. However, the Cotton-Mouton interferometer at 118 μm remains a viable option for use in the divertor region. Potential problems with this approach are: (1) perpendicular alignment to B_T is critical and must be maintained. Any misalignment could result in large phase shift from the Faraday effect. Since B_T is so large for ITER, the Faraday effect would be significant for even a 1-deg misalignment (see previous discussion). (2) The 1-2 cm toroidal gap available in the divertor cassette for the source radiation appears too small for use with laser radiation at 118 μm. This small gap makes the use of waveguide unfeasible in the cassette region. Free space propagation using focusing optics also appears marginal. Consequently, the divertor cassettes would need to be re-engineered to provide more space, say 3-4 cm, in order for the long wavelength Cotton-Mouton polarimeter option to be viable. (3) Polarization integrity must be maintained when making a C-M measurement. Any beam interaction with the walls of the toroidal gap could act to distort the polarization. This again indicates the need for a wider toroidal gap. In the 2005 Divertor interferometer Report [1], refraction was listed as a potential issue for wavelengths longer than 10.6 μm based on a rough estimate assuming the density gradient was everywhere constant across the divertor leg. More accurate refraction calculations using a ray tracing code have been made in the ITER divertor region that show that refractive effects are manageable at both 57 ands 118 μm. This is true even for the maximum density case (Sec. 3.3) although fast transient events associated with ELMs may still be problematic.

3.1.4. Differential Interferometer

A differential interferometer measures the phase difference between a pair of closely spaced interferometer chords at nearly the same wavelength ($\Delta\lambda/\lambda \approx 10^{-6}$) [13]. Both chords experience essentially identical optics and are mixed in a single detector so that vibration effects cancel. The phase difference can be adjusted to be less than a fringe (by adjusting the spatial separation of the two chords) making the fringe skip problem negligible. In plasmas with closed flux surfaces where density profile inversion is needed, the differential interferometer provides identical information to a conventional interferometer without requiring vibration compensation and without fringe skip errors. However, in the divertor region the flux surfaces are not closed thereby preventing density inversion. In this situation, the line-integrated density measurement would have to be extrapolated from a differential interferometer measurement that reduces the overall accuracy (of the inferred line-integrated density measurement). Furthermore, the differential interferometer requires an estimated ~2 cm spatial separation of two beams for the ITER divertor to meet required phase accuracy. This makes sharing common optics more problematic and reduces vibration/thermal expansion compensation. The differential interferometer has a limited application in divertor region unless a large number of closely spaced chords are employed. Differential interferometry using a single CCR (double pass measurement) is not feasible in the divertor. A limited version of differential interferometry may have application by using adjacent corner cube reflectors (spacing ~3 cm) if the CCRs were mounted on the same structure and experienced the same thermal expansion/vibration.

3.1.5. Dispersion Interferometer

In its simplest form, conventional two-color interferometry measures a phase shift due to the plasma plus vibrations (or thermal expansion, etc.) using two separate wavelengths that make independent measurements. This allows one to isolate the phase shift due solely to the plasma. Typically, the total phase measured at each wavelength is much greater than a fringe for both the plasma and vibration contributions. This leaves two-color systems vulnerable to fringe counting errors.

Dispersion interferometry [14] (DI) also employs two colors to make the plasma phase measurement but has the highly desirable feature that the vibration effects cancel before making the phase measurement. Instead of making independent measurements at each color (using separate detectors, amplifiers, fringe counting electronics, etc. like the two-color interferometer), DI employs a single detector and measures the phase between

the two colors directly. Since the two colors are λ and 2λ, harmonic generated by using a frequency doubler, the thermal expansion effects cancel out along the entire beam propagation path. This makes the DI only vulnerable to fringe counting errors due to the plasma phase shift. For the ITER divertor, plasma induced phase shifts are nearly always $<2\pi$ when using 10.6 μm (exceeds 2π only for the highest density case and then by only a relatively small amount). Consequently, implementation of DI techniques in the ITER divertor offers the possibility of eliminating fringe-counting errors. In this regard, it is encouraging to note that recent results on TEXTOR [8] employing this technique demonstrate its effectiveness and show sensitivity of $\langle n_e l \rangle_{min} \sim 2x10^{17}$ m^{-2}. These results exceed accuracy requirements for the ITER divertor as mentioned earlier. Potential limitations of the DI approach are the frequency doubler efficiency (which is currently $\sim 7x10^{-5}$) and the limited bandwidth obtained in the initial implementation on TEXTOR.

3.2. Sources, Detectors, Optics Technology

The conclusion of this report is that 10.6(5.3) μm two-color interferometer is recommended as the optimum approach for measuring density in the ITER divertor region. The fusion community has extensive experience in this region of the spectrum and the interferometers have proven performance. In addition, high quality sources, detectors and other optical components are commercially available at these wavelengths. Infrared CO_2 lasers, associated detectors, and optics are used widely in the industrial, medical, and scientific communities. Typical CO_2 lasers used for fusion plasma diagnostics (e.g., interferometry) are grating tuned waveguide lasers in the 1-10 Watt category operating at 10.59 microns. At this power level, sufficient signal can be obtained from room temperature photovoltaic or photoconductive HgCdTe detectors.

Less commonplace than CO_2 are CO lasers; however, several manufacturers for CO lasers exist (e.g., Infrared Instruments, San Marcos, CA USA; Access Laser Co., Marysville, WA USA; Edinburgh Instruments Ltd. Scotland). The typical lasing line used for the CO molecule is at 5.27 μm. Many of the CO laser manufacturers use the same exact technology as that employed for their CO_2 lasers and as a result similar beam quality, line width, etc. can be expected. Peak power levels are typically less than the comparable CO_2 laser (1-10 W) and are in the range of 0.1–1.5 W. At the shorter wavelength, however, several other detector options exist with much higher gain (10-100x) than those used for the 10.59 μm CO_2 line — more than making up for the lower power. Even the same detectors that are used for 10.59 μm exhibit 2-3 times the sensitivity at 5.27 μm [15].

Several materials exist which have acceptable transmission and are suitable for optical components or windows at both 10.59 and 5.27 μm. Typical options include ZnSe, BaF_2 and CVD diamond. Common transmissive optical components such as beam splitters will likely be made from ZnSe due to low cost and availability while windows will be made out of either BaF_2 or CVD diamond due to their lower Verdet constants with CVD diamond the forerunner due to durability (Verdet constant of BaF_2 is unknown but similar materials have Verdet constants an order of magnitude smaller than ZnSe). Taking advantage of this lower Verdet constant, CVD diamond windows have been used with great success on the JT60-U tokamak with the almost complete elimination of extraneous Faraday rotation previously observed using ZnSe windows [16]. CVD diamond has the added benefit of a very similar index of refraction at 5.27 and 10.59 μm $|\Delta n/n| < 4\text{x}10^{-4}$, $n \sim 2.376$ [17]. This matched index of refraction will help to eliminate uncompensated phase shifts due to motion across a wedged window surface.

A longer wavelength source choice would be a CO_2 pumped molecular gas laser with output at 57 and 48 μm. The only known development work at 57 and 48 μm is being carried out in Japan. Laser sources have been developed showing output powers up to 1.6(0.8) W at 57(48) μm [18]. In addition to source development work, an interferometry-polarimetry diagnostic using this laser has been bench tested and is being modified for use on the LHD stellarator [19]. Progress of this work should be monitored in the future. Source, detector and diagnostic development at these wavelengths may also have potential relevance to the ITER TIP system.

3.3. Refraction

In the 2005 Report of the ITER Divertor Interferometer [8], a rough estimate of refractive effects at various wavelengths indicated that longer wavelengths of 57 and 118 μm were potentially susceptible to significant beam path deviations due to large transverse density gradients. The estimate provided was crude and was based on assuming that the density gradient was constant along the beam path, thereby providing an upper bound estimate. This issue has now been addressed by using a ray-tracing code developed for the open field line configuration of the divertor and using the simulated ITER divertor density profiles (Fig. 2). The assumption of constant transverse density along the chord was dropped. Details of the approach used for the ray tracing and analysis results are provided in Appendix A.

As an example, the results of running this code at long wavelength λ=118 μm for the high-density divertor scenario, ($n_{e0} = 1\text{x}10^{22}$ m^{-3}), are shown in Figs. 11 and 12. This is

the worst-case scenario since we've chosen the longest wavelength considered for the divertor and the highest density. For the eight different beams paths considered (Fig. 1), the vertical beam displacement after a single pass (evaluated at the corner cube reflector located ~35 cm from the plasma) ≤1.5 mm. For shorter wavelengths of 57 and 10.6 μm, this displacement is reduced, going as λ^{-2}, to <0.35 and <0.01 mm, respectively. For radiation at 10.6 μm, the estimated corner cube reflector size is 15 mm x 25 mm (would be larger for longer wavelengths), making the beam displacements due to refraction negligible at 10.6 μm. Beam path length changes are also small compared to a wavelength in each case, as shown in Fig. 11, implying a small or negligible phase correction. Similar results except for the case of interferometer sightlines perpendicular to the divertor leg are shown in Figs. A-3 and A-4.

The ray-tracing results are significantly smaller (when including geometrical effects) than the original estimate implying that refraction is no longer a reason for eliminating use of longer wavelengths (either 57 or 118 μm) in the ITER divertor. This stems largely from the fact that the 2005 report took the density gradient to be constant along the chord (~30-40 cm, giving an upper bound as stated in the report) when in reality it would have been more accurate to take the density gradient as a constant for the divertor density filament width (~2 cm). It should be noted, however, that if a MARFE [20] were to appear in the divertor or if a transient ELM event occurred, it is likely that the density gradients will steepen and refraction will increase. The ray-tracing results herein only deal with the high-density divertor scenario provided by the ITER team.

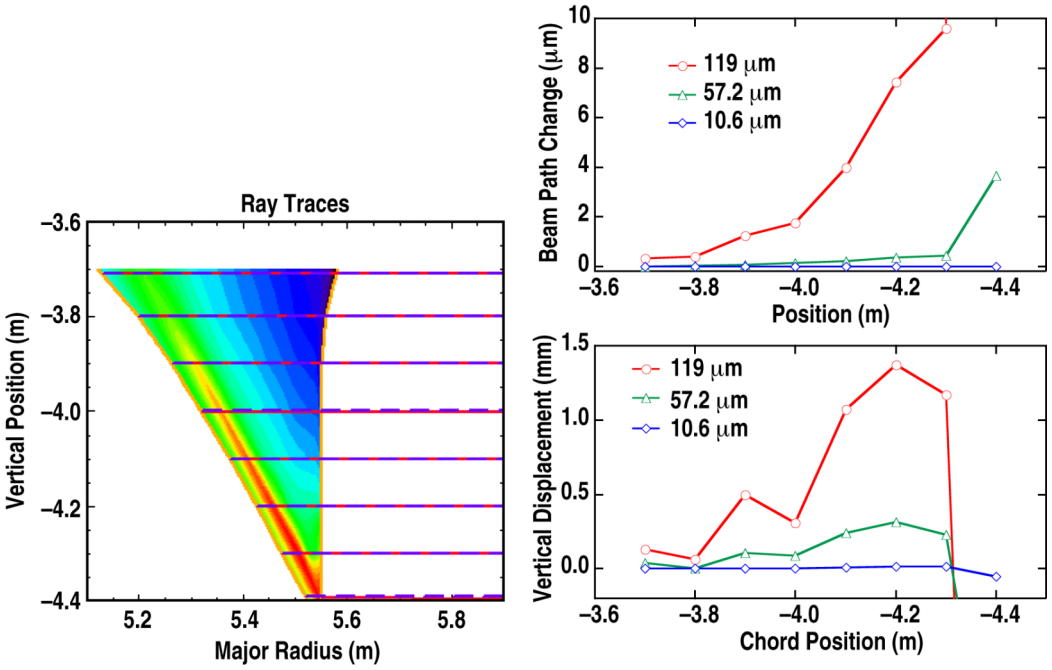

Fig. 11. Ray tracing results using horizontal chord paths for the highest density divertor scenario, n_{e0} = 1x10^{22} m^{-3}. Vertical displacement and beam path change are evaluated at CCR located 35 cm from plasma.

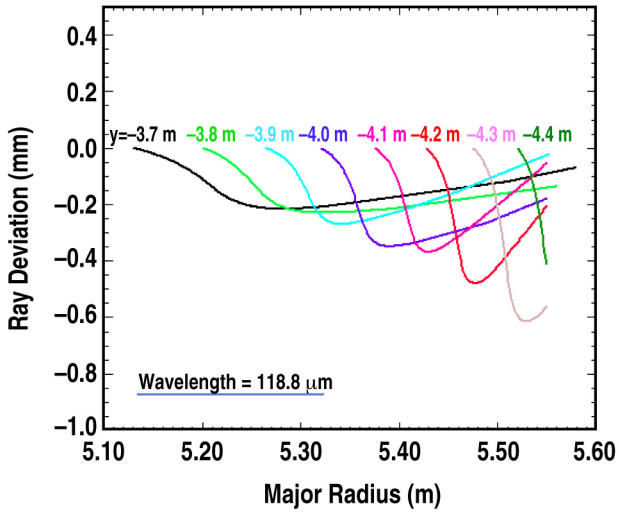

Fig. 12. Ray deviation for each chord at λ = 118.8 μm using horizontal chord paths.

4. SYSTEM ALIGNMENT

A realtime feedback alignment system will be necessary to maintain alignment of the divertor interferometer due to the thermal expansion and movement of the ITER vessel. In principle, the design presented by Carlstrom, *et al*. [21] should be adequate. It involves using a portion of the probing beams (via beam splitters) and quadrant detectors (e.g., room temperature quadrant detectors from Vigo System PCQ series or liquid N_2-cooled detectors from Judson Technologies, J15QUAD series) to determine the position of the laser beams (Fig. 13). The difference between the measured position and the desired position is then used in a feedback loop to control a steering mirror upstream of the detector. The retro-reflectors (CCR) automatically maintain the angular alignment of the laser beams. If necessary, the final beam combiner can be dithered to maintain the maximum interference signal on the detector.

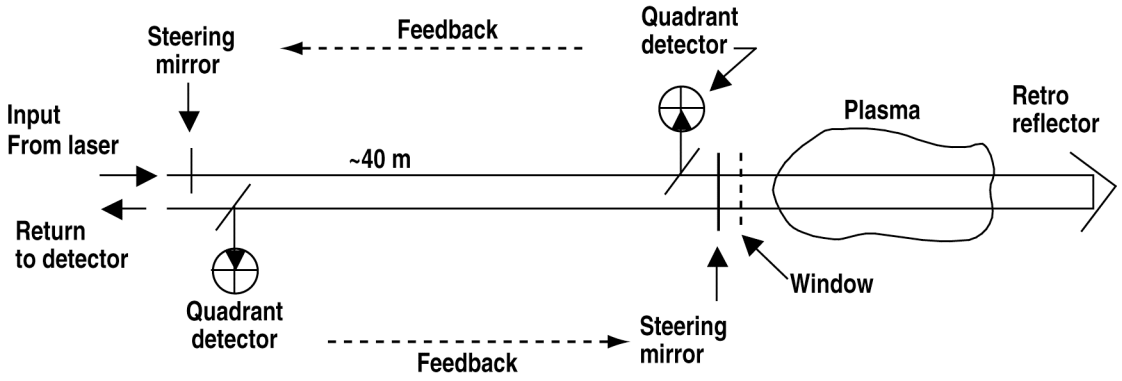

Fig. 13. Feedback alignment system using two feedback loops.

As an alternative to the quadrant detector approach, gradient search algorithms based on a single detector output are commonly used. In fact, several companies offer integrated motion control solutions ideally suited to this type of feedback alignment problem which utilize gradient search techniques. For example, Thorlabs' PC-based "APT NanoTrak" system can support several modules each of which is capable of controlling a two-axis piezo actuated mirror, with up to 300 Hz time response. We recommend that a feedback alignment system prototype be developed as a research and development task for the divertor interferometer system.

5. MIRRORS

Mirror damage issues in the divertor region are in many ways similar to those for TIP and poloidal polarimetry systems. Simulation of environmental effects on retro-reflectors in ITER was reported by Voitsenya, *et al*. [22]. They discuss two effects that may be detrimental to plasma facing mirrors; sputtering by charge exchange neutrals and deposition of carbon-based (or beryllium-based) contaminant layers. Sputtering erodes the surface and can change a smooth reflective surface into diffuse scattering surface. It also can lead to changes in the polarization ellipse of the reflected signal and affect polarization measurements. However, the effect of sputtering can be significantly reduced by placing the mirrors behind long collimating apertures that reduce the exposure solid angle of the mirrors to the plasma. For example, the 2.5x1.5 cm retro-reflectors depicted in Fig, 5 can be placed behind 35 cm long collimators that will reduce the solid angle from π to 0.0008, a factor of 4000. This should reduce the role of erosion significantly. If one uses the upper limits of sputtering to be 5 μm (as estimated for the poloidal polarimetry system [20]), the expected sputtering removal should be down to ~4 nm, which will have a negligible affect on even the shortest 5.27 μm interferometer performance. In fact, 1-2 orders of magnitude more sputtering could be tolerated. This analysis assumes space availability for such an extended collimating structure. From Figs. 1, 7 and 8, this appears feasible, however, the actual space limitations will have to be clarified. The choice of mirror material can also minimize the effects of sputtering, with tungsten, rhodium, and molybdenum having acceptably low sputtering removal rates.

Deposition of carbon-based (or beryllium-based) contaminant layers can reduce the reflectivity of the mirror surface and lead to changes in the polarization ellipse of the reflected signal. This is a difficult problem to analyze because there are not sufficiently developed models to predict the deposition rates. Anecdotal evidence from TEXTOR and Tore Supra, both limited tokamaks, suggest that deposition may be a problem at wavelengths of 10 μm or less. However, evidence from DIII-D, an all graphite, diverted tokamak, shows that a corner cube reflector mounted on the inside wall survives very well, even at 3.39 μm with little degradation of interferometer performance after several years of operation. In an experiment to measure the deposition rate of carbon on molybdenum mirrors in the divertor of DIII-D, Rudakov, *et al.* [23] showed that heating the mirror surface greatly reduced the amount of deposition. We expect that placing the mirrors behind long collimating apertures to reduce the solid angle and heating the mirrors to reduce deposition will mitigate mirror damage problems. The baseline design

called for cooling the mirrors to avoid thermal distortion. Taking advantage of this, one can pick an appropriate temperature to reduce the deposition rates.

6. CRITICAL R&D NEEDS

1. Divertor interferometer prototype using two-color interferometry (10.6/5.3 μm) (laboratory test and plasma test).
   - Investigate second harmonic interferometers; their robustness, phase noise, ease of operation, and suitability for ITER.
   - Minimize phase noise and optimize time response. Verify (in)sensitivity to path length changes. Optimize phase resolution electronics.
   - Test components such as lasers, detectors, AO cells, optical components, beam splitter with good polarization characteristics, etc.
   - Evaluate effects (if any) resulting from large neutral gas population in the divertor.
   - Evaluate refraction effects due to fast transient events such as ELMS
   - Prototype beam paths in the divertor using real spatial constraints.
   - Investigate the use of waveguides and/or optical fibers.
2. Prototype and test realtime feedback alignment system.
3. Design, build, and test temperature controlled mirrors and retro-reflectors.
4. Integrate interferometer space requirements with overall divertor cassette design.

7. SUMMARY

In summary, a two-color interferometer using laser radiation at 10.6(5.3) μm appears to be the best option for the ITER divertor. The phase resolution of such a system is sufficient for the baseline and higher density divertor scenarios and the total plasma-induced phase shift is <1 fringe. The short wavelengths are less susceptible to fringe counting errors and refraction (which can potentially be large during ELMs and MARFEs). Source and receiver technology is readily available. In addition, free space propagation techniques can be used to transport the beam to the machine from the diagnostic hall as well as within the vacuum vessel and divertor cassette while maintaining beam dimensions that are compatible with the severely restricted space between the cassettes. Longer wavelength options, while having better overall resolution, suffer from multiple plasma-induced fringes (susceptible to fringe counting errors) and larger beam (and associated optics like the CCRs) dimensions that conflict with present space constraints in the toroidal gap. Use of over-moded waveguide techniques to transport the beam can potentially be used outside the divertor cassettes (i.e., from the diagnostic hall to the device) but appear incompatible with the 1-2 cm toroidal gap constraint. In addition, feedback alignment to waveguide requires keeping the beam on the same optical axis presenting a more severe constraint than for free space propagation. Source and receiver technology at 57/48 μm is also limited.

1. With possible beam diameters of ~0.5 cm over a several meter range, 10.59 μm CO_2 systems provide an attractive option in the divertor region where access is extremely limited (less than 2 cm in the toroidal direction).

2. Refraction and fringe rates are less severe (for transient plasma events) for 10.6 μm than for 57 μm or longer wavelength systems.

3. For the specified resolution requirement of 20%, the minimum nL of 1.7×10^{19} m^{-2} for the baseline density scenario implies a resolution of 3.4×10^{18} m^{-2}, which is satisfied by a 10.59/5.3 μm system. A two-color interferometer with this wavelength combination is capable of 1.2×10^{18} m^{-2} at 1-degree phase resolution (electronics are capable of <0.1 degree if other sources of noise can be controlled).

4. Real-time density information is available.

5. The fusion community has experience using 10.6 μm systems and they have proven performance.

6. A dispersion interferometer at 10.6 μm would be less susceptible to fringe skips for most of the operating density ranges because the plasma phase shift is $< 2\pi$.

7. Fringe skips for a two-color system will be minimized by using a feedback alignment system and high-speed electronics.

8. Fringe skips, if they do occur, can be compensated for in realtime by using software as presently done on JET.

9. Mirror damage can be mitigated by placing mirrors behind long, high aspect ratio shield tubes and controlling their temperature to minimize deposition.

10. Corner-cube reflectors (double pass measurement) are necessary to maintain alignment.

11. A feedback alignment system is required.

REFERENCES

[1] R. Prentice, *et al.*, Rev. Sci. Instrum. **66**, 1154 (1995) and G.M. McCracken, *et al.,* Nucl. Fusion **38**, 619 (1998).

[2] R.A. James, *et al.,* Rev. Sci. Instrum. **66**, 422 (1995).

[3] Divertor ITPA Topical group recommends 2 cm resolution required near the target plate; Private discussion with George Vayakis.

[4] USIPO Statement of Work document states that currently six chords are planned for the outer leg and four for the inner leg.

[5] Jean Pierre Crenn, IEEE transactions on Microwave Theory and Techniques, **MTT-27**, 573 (1979).

[6] G. Vayakis, ITER_D_24HYZK 2.0 (2006).

[7] N. Bretz, F. Jobes and J. Irby, Rev. Sci. Instrum. **68**, 713 (1997).

[8] D.L. Brower, Report on *Conceptual Design Study for ITER Divertor Interferometer*, December 2005.

[9] D.L. Brower, W. Ding, B. Deng, Rev. Sci. Instrum. **77**, 10E911 (2006).

[10] P.A. Bagryansky, *et al.,* Rev. Sci. Instrum. **77**, 053501 (2006).

[11] P. Innocente, D. Mazon, E. Joffrin, M. Riva, Rev. Sci, Instrum. **74**, 3645 (2003).

[12] A. Murari, L. Zabeo, A. Boboc, D. Mazon, M. Riva, Rev. Sci. Instrum. **77**, 073505 (2006).

[13] W.X. Ding, D.L. Brower, B.H. Deng, T. Yates, Rev. Sci. Instrum. **77**, 10F105 (2006).

[14] V.P. Drachev, *et al.,* Rev. Sci. Instrum. **64**,1010 (1993).

[15] www.vigo.com.pl, www.boselec.com/products/detir.html

[16] Y. Kawano, S. Chiba, A. Inoue, Rev. Sci. Instrum. **75**, 279 (2004).

[17] D.F. Edwards, E. Ochoa, J. Opt. Soc. Am. **71**, 607 (1981).

[18] K. Kawahata, *et al.,* Rev. Sci. Instrum. **75**, 3508 (2004).

[19] T. Akiyama, K. Kawahata, *et al.,* Plasma and Fusion Research **1**, 001 (2006).

[20] B. Lipschultz, *et al.,* Nucl. Fusion **24**, 977 (1984).

[21] T.N.Carlstrom, *et al.*, "Baseline design of a multi-channel interferometer and polarimeter system for density measurements on ITER" *Diagnostics for Experimental Thermonuclear Fusion Reactors 2* Edited by Stott *et al.*, Plenum Press, New York, 1998.

[22] V.S. Voitsenya, *et al.,* Rev. Sci. Instrum. **76**, 083502 (2005), and Rev. Sci. Instrum. **72**, 475 (2001).

[23] D.L. Rudakov, *et al.,* Rev. Sci. Instrum. **77**, 010F126 (2006).

APPENDIX A: RAY TRACING FOR ITER DIVERTOR INTERFEROMETER

Procedures to calculate the beam refraction for ITER divertor interferometer are as follows. First, 2-D density distribution over the divertor area (2-D grid points) is obtained from the given eight-chord radial density distribution data. To ensure the accuracy of ray tracing, spatial resolution of 1 mm horizontally (radially) and 2 mm vertically are used.

Ray tracing proceeds at a horizontal step size of about 1 mm. Rays impact the plasma from small major radius side going to large major radius side, at a given angle of propagation (horizontal or perpendicular to the filament). Once contact is made with the plasma boundary, the plane normal to the density gradient direction is the interface, the angle between the density gradient and the incident ray is the incident angle, and the refractive index before the interface is 1. The plasma boundary density at the point of contact is used to calculate the refractive index after the interface. The refraction angle and the refractive ray direction, are then obtained from Snell's law.

Subsequently, the ray is brought one step forward at this new direction inside the plasma. At this new position, the plasma density and gradient are obtained from the interpolated values. The plane normal to the density gradient direction is the interface, the angle between the density gradient and the incident ray is the incident angle. The density before the interface is calculated by subtracting the density increment from the interface density, where the density increment is calculated from the density gradient and half the displacement from previous ray point to the new interface. The density after the interface is the sum of the density increment and the interface density (Fig. A-1). The refractive indices before and after the interface are then calculated from the densities for the application of Snell's law. The refraction angle and the refractive ray direction are subsequently obtained. This process is repeated until the plasma boundary is reached, and the beam deviation as well as the beam path length change are then calculated by comparing the actual ray trajectory and the straight line at the initial incident angle (Fig. A-2).

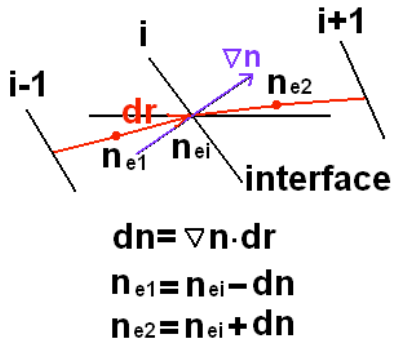

Fig. A-1. Applying Snell's law at the i-th interface.

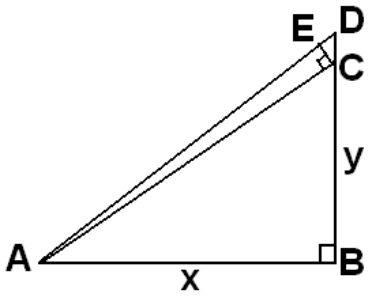

Fig. A-2. Geometry: AC is a straight line at the initial incident ray direction, AD is the actual (refracted) ray, EC is the transverse beam deviation (called vertical displacement in the figures), and AE-AC is the beam path length change.

As an example, the results of running this code at long wavelength λ=118 μm for the high-density divertor scenario, ($n_{e0} = 1\times10^{22}$ m^{-3}), are shown in Figs. A-3 and A-4. This is the worst-case scenario since we've chosen the longest wavelength considered for the divertor and the highest density. For the eight different beams paths perpendicular to the divertor leg (Fig. A-3), the vertical beam displacement after a single pass (evaluated at the corner cube reflector located ~35 cm from the plasma) ≤ 1.1 mm. For shorter wavelengths of 57 and 10.6 μm, this displacement is reduced, going as λ^{-2}, to <0.2 and <0.01 mm, respectively. For radiation at 10.6 μm, the estimated corner cube reflector size is 15 mm x 25 mm (would be larger for longer wavelengths), making the beam displacements due to refraction negligible at 10.6 μm. Beam path length changes are also small compared to a wavelength in each case, as shown in Fig. A-3, implying a small or negligible phase correction. The ray deviation as a function of major radius is shown in Fig. A-4, where the ray deviation is defined as line segment EC in Fig. A-2. These beam deviations are extrapolated to the corner cube reflector positions 35 cm from the plasma boundary to obtain the vertical displacement shown in Fig A-3.

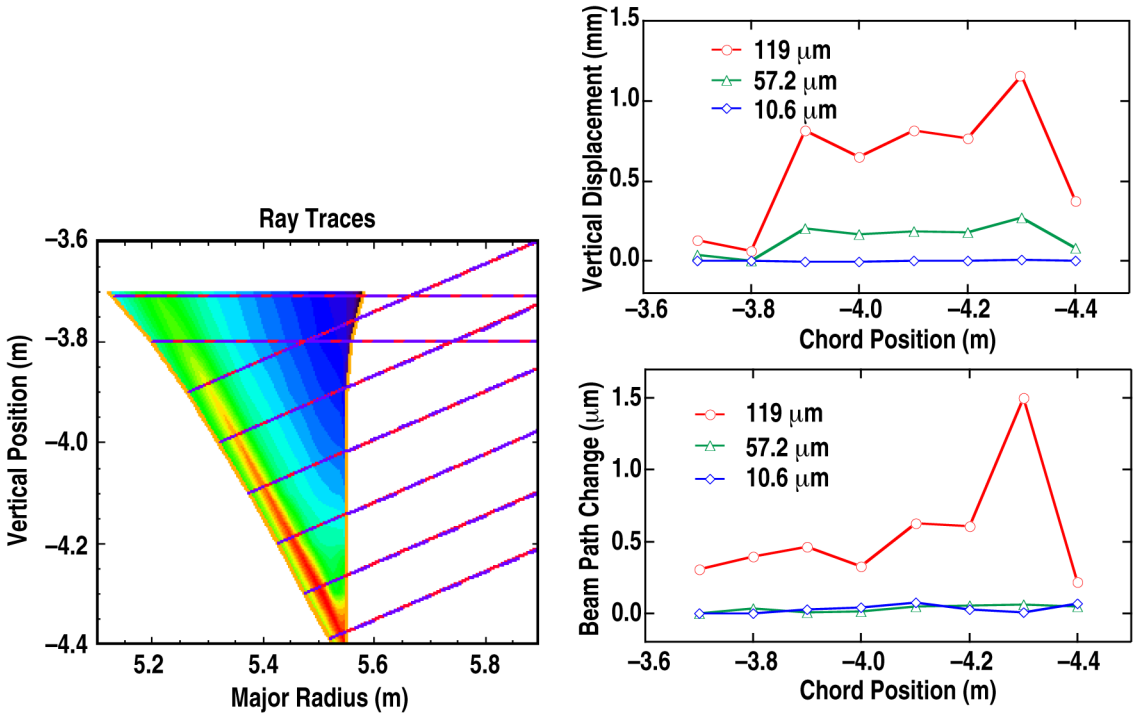

Fig. A-3. Ray tracing results using chord paths perpendicular to the divertor leg for the highest density divertor scenario, n_{e0} = 1x10^{22} m^{-3}. Vertical displacement and beam path change are evaluated at CCR located 35 cm from plasma.

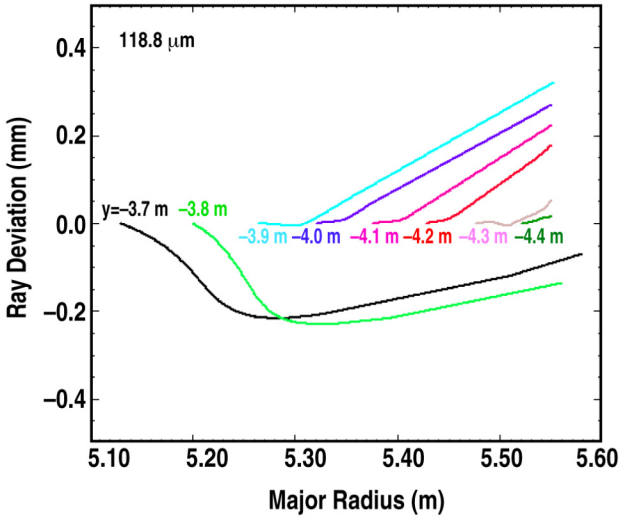

Fig. A-4. Ray deviation (EC) for each chord at λ = 118.8 μm, with the beams incident perpendicular to the divertor leg.

APPENDIX B: STATEMENT OF WORK

Listed below are the specific work tasks to be performed under this statement of work.

3.1. Consider the reference design and the significant changes proposed for it in Ref. 1.3.3. Make specific recommendations for the choice of wavelength(s) taking account of the expected plasma characteristics and the available space. Evaluate the benefits of applying different interferometer techniques including the Cotton-Mouton Effect and differential interferometry. Sections 1, 2 and 3

3.2. The final choice of wavelengths to be used may depend on developments of available sources and detectors. If necessary, travel to sites where the developments are being carried out (probably Japan). Equally important, a full understanding of the space allocation and access to the divertor and port structure will be facilitated by discussions with the US design team working on port L8 and with the ITER central team. Sections 3.2 and 2

3.3. Develop the initial optical path design compatible with the overall allocation of space and identify the use of waveguide and/or focusing optics, justifying the choice for the transmission approach. Section 2

3.4. Carry out ray tracing analyses to identify and resolve issues of refraction. Sections 3.3 and A-1

3.5. Determine the need for active alignment of the different channels, and develop a concept for alignment control. Section 4

3.6. Address the issues of deposition and erosion of first mirrors and/or corner cubes in the divertor and propose geometric locations and techniques to mitigate the impact. Section 5

3.7. Identify critical R&D needs. Section 6

3.8. Present summary of findings and provide electronic copy of presentation at USIPO/BPO workshops and/or ITPA Diagnostic TG meetings.